An Image Processing System for Automated Quantitative Analysis of Hummingbird Flight Kinematics

Michael McKinley Medical Imaging Spring 2010

Abstract

In this work, an image-processing system for quantitative analysis of hummingbird flight kinematics was developed, implemented, and tested. The system applies a number of normalization, thresholding, and edge detection algorithms to automatically analyze high speed video. This algorithm functions as a tool for researchers to quickly ascertain a multitude of information pertaining to the kinematics of flying hummingbirds. Parameters of interest include wing beat frequency, wing angle of attack, body pitch, and wing stroke amplitude. This system can be applied to similar problems where video images can be used as a rapid analysis tool.

Introduction

Determining hummingbird flight kinematics has been the subject of numerous research initiatives [1]. Recently, engineers have become increasingly interested in the flight capabilities of these animals, as they are capable of tightly controlled flight when subjected to large disturbances. One widely used method for studying hummingbird flight is to place the animals in the working section of a wind tunnel (see Figure 1). The enclosed region of a small wind tunnel (3'x3'x3' working section) is an ideal environment for studying flight characteristics, as high speed video cameras can be easily trained on the animals from many perspectives (see Figure 2). Typically, after capturing a high speed video, flight parameters (beat frequency, wing angle of attack, body pitch, and wing stroke amplitude see Figure 3 and Figure 4) are measured by hand. This procedure requires researchers to tediously hand measure flight parameters using image analysis software (typically 30-45minutes of work per video). As a result, researchers must allocate a substantial amount of time to processing video. The image processing system developed in this work achieves the same measurement objectives in a single automated process. Furthermore, automation furnishes the possibility to include uncertainty measurement and automated data statistics. The processing system can be automated to process batches of data and thus increase work efficiency.

System Overview

Image analysis is performed in several serial operations. Two orthogonal high resolution high speed cameras (1280x1040 resolution at 500 fps) are trained on the interrogation region of the wind tunnel see Figure 5. By having two orthogonal images, it is possible to calculate three-dimensional kinematics of the flying animals. Additionally, a second data stream affords an additional measure of system robustness. As hummingbirds are obligate nectavores, capturing steady state flight video is a simple matter of waiting for the animal to feed. The raw video stream from both cameras is uploaded into MATLAB for further analysis (see Figure 6). Note that the frames captured in these videos have a relatively small depth of field relative to the wind tunnel dimensions. This property will simplify further analysis, as foreground objects question will be in sharp focus relative to background objects.

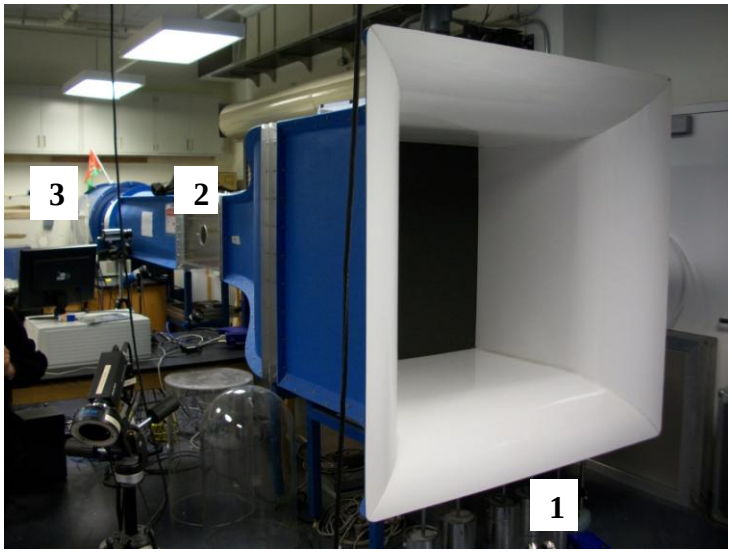

Figure 1 -Wind tunnel. 1) Inlet, 2) Working section, 3)Outlet.

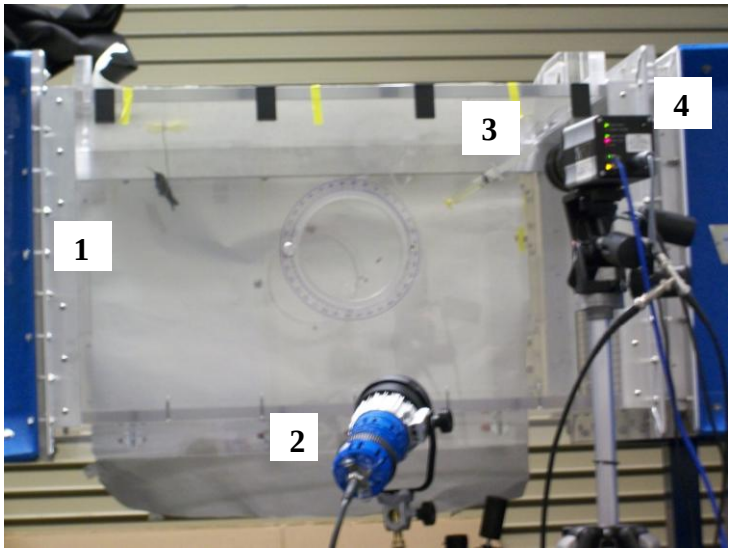

Figure 2 - Working section of wind tunnel. 1) Anna's Humming bird, 2) DC halogen light source, 3) Humming bird feeder, 4) Side view camera.

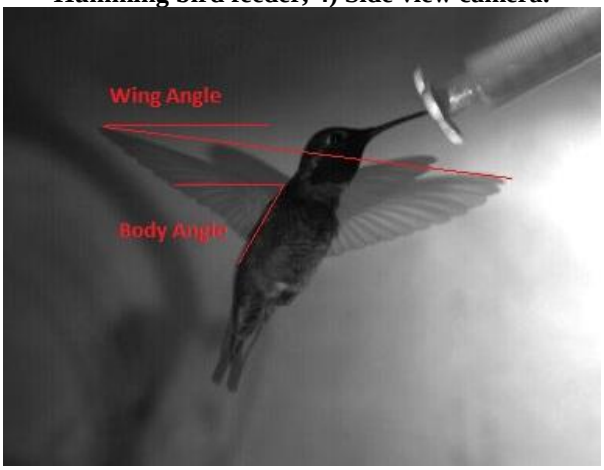

Figure 3 - Angles measured from the side view

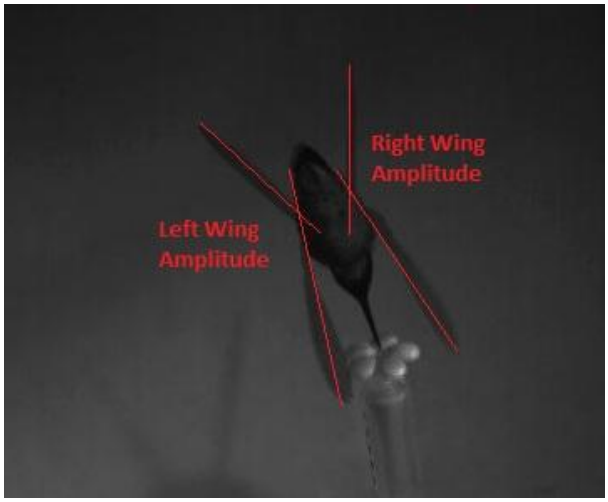

Figure 4 - Angles measured from the bottom view

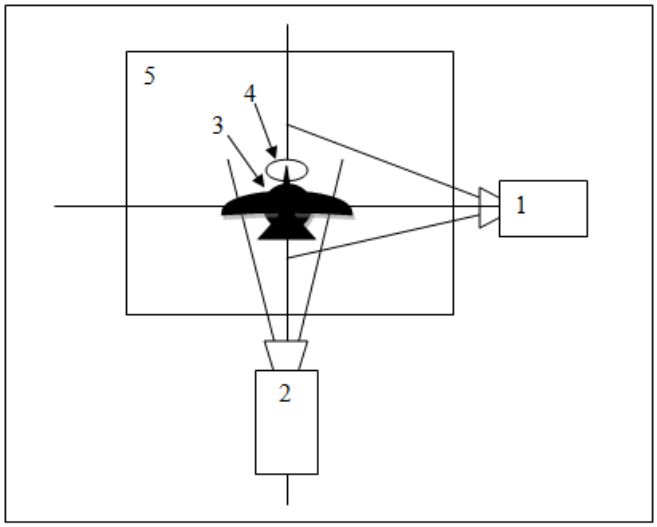

Figure 5 - Diagram of wind tunel test setup. 1) Side view camera, 2) Bottom view camera, 3) Hummingbird, 4) Feeder, 5) Boundaries of wind tunnel working section

Calculation of wing beat frequency

An initial background subtraction is performed on both video streams using the frame difference method. As illustrated in Figure 7, the frame difference background subtraction highlights regions of large variation between frames. The bird's illuminated wingtips provide a metric for measuring visible wing area throughout each video. Note that this background subtraction process leaves us with some noise to be addressed in subsequent operations (upper right hand corner of Figure 7). Fortunately, the large scale noise visible in these images is directly correlated to wing movements (wing shadows, reflections etc…). In order to calculate beat frequency, we will be observing the rhythmic change in visible wing area through an entire wing beat cycle. Noise correlating to wing beats will strengthen the wing beat signal, and will not be removed until subsequent operations. To get a rough idea of visible wing area in each frame, a threshold operation is performed on each background subtracted frame, and white pixels (corresponding to wings) are counted in each image. the thresholding operation is performed across the entire range of possible threshold values (see Figure 8), rather than selecting an arbitrary threshold value. White pixel area for each frame is summed across the entire threshold range to produce the wing beat signal illustrated in Figure 9, a plot of visible wing area as a function of time. A fast Fourier transform (FFT) is performed on the time varying signal of visible wing area as a function of time to determine the signal spectrum.

This process (import video, background subtract, threshold, sum white, FFT signal) is performed on both video perspectives to produce two spectral analyses. The frequency spectrum produced for each video can be added to produce a spectrum with better signal to noise characteristics as illustrated in Figure 10. It is possible to pick the dominant wing beat frequency after eliminating the DC component from the spectral analysis with a simple high pass filter. It should be noted that spectral power peaks are present at the dominant beat frequency f_beat, and higher frequencies f_beat * N (where N is an integer). See Figure 21 for a flowchart of the beat frequency calculation process.

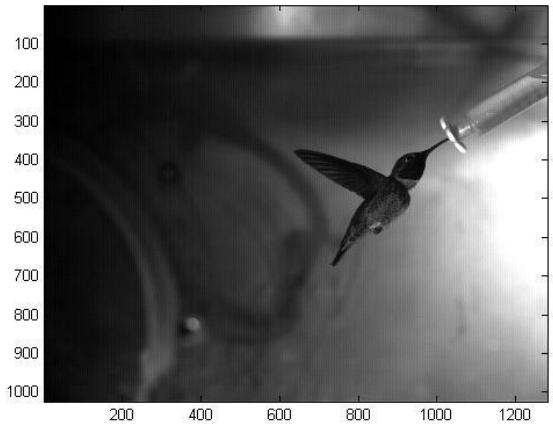

Figure 6 - Raw video frame imported into MATLAB

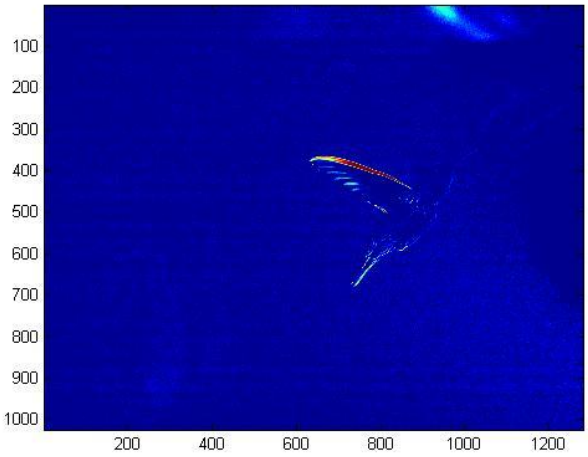

Figure 7 - Background Subtraction. Note noise in upper right hand corner correlating with shadow of bird.

Figure 8 - Range of thresholded side images (L to R, High threshold, Low threshold)

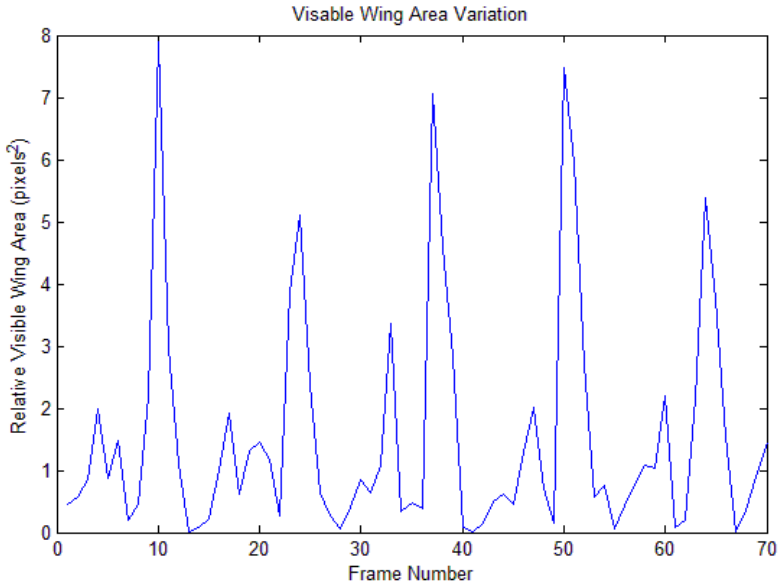

Figure 9 - Summation of white area across all thresholds at each frame (revealing wing beat cycle)

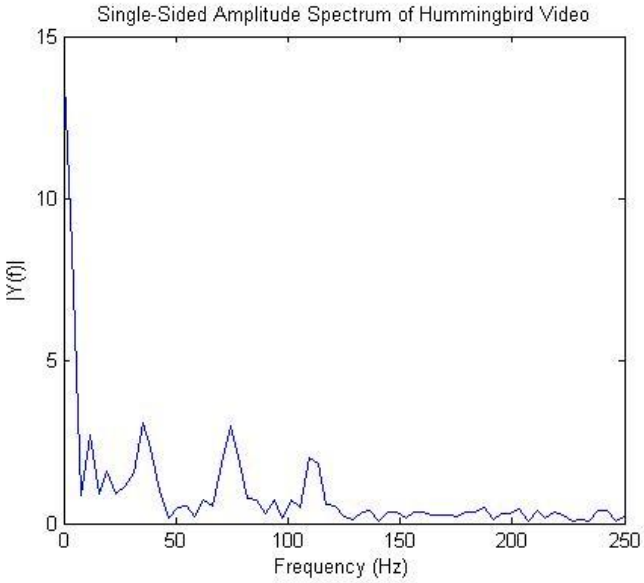

Figure 10 - FFT of wing beat signal (reveals dominant frequency f_beat at 38.5 Hz and secondary peaks at f_beat*N)

Calculation of wing stroke amplitude

See Figure 4 for a graphical representation of wing stroke amplitude as defined in the literature [3]. Bottom view images (background subtracted and thresholded from the previous operation of beat frequency calculation) are utilized for wing stroke amplitude calculation (see Figure 11). Each frame is eroded and dilated to eliminate noise (compare noise reduction between Figure 11 and Figure 12). Blob detection is performed at this stage to locate the primary points of interest, centroids and orientations of each blob are calculated (Figure 12). As illustrated in Figure 13, Prewitt edge detection is performed on the raw image. The edge profile is laid over the blob detected regions and blobs outside of the detected edges are eliminated. This process subtracts all additional sources of noise, and leaves only blobs associated with the wing profile. Centroids of blob trajectories are tracked in subsequent frames to eliminate the effect of occlusions, and to help identify associated blobs in subsequent frames. Orientations of blobs at extreme wing trajectories are identified, and wing stroke amplitude is calculated by taking the inverse cosine of the dot product between these two vectors. Wing stroke amplitude is calculated for a number of consecutive wing beats to provide an average and standard deviation of this parameter. See Figure 22 for a flow chart of the stroke amplitude calculation process.

Figure 11 - Thresholded bottom view image after background subtraction

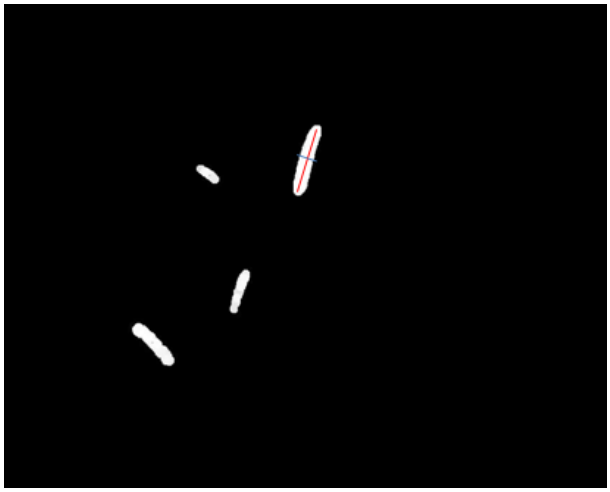

Figure 12 - Bottom image after erosion, dilation, and blob detection. Note centroid and fitted ellipse axes (red and blue lines).

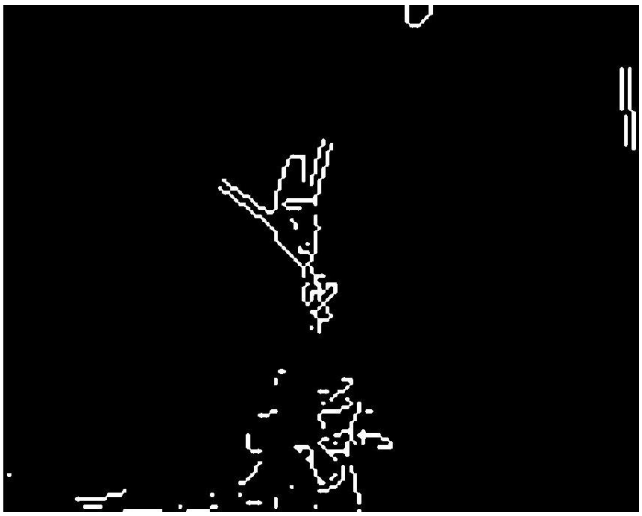

Figure 13 - Prewitt edge detection of raw bottom image

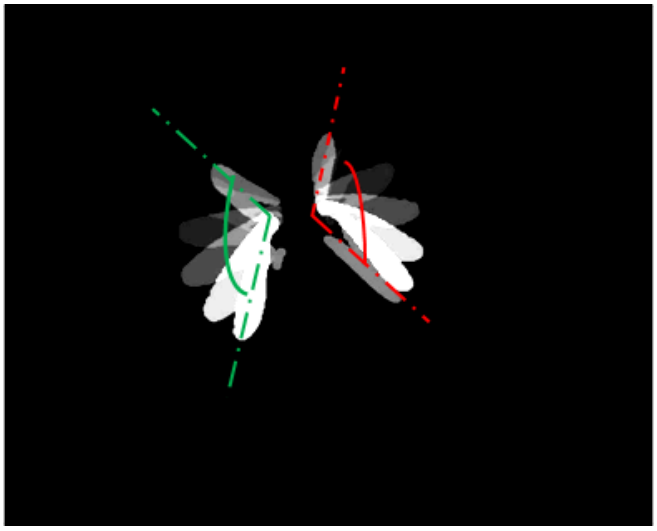

Figure 14 - Extraneous blobs (outside edge detected region) removed. Blobs tracked, and angles measured for left and right wings.

Calculation of wing stroke angle

Determining wing stroke angle is a similar process to calculating wing stroke amplitude. See Figure 3 for a graphical representation of wing angle as defined in the literature [4]. Side view images (background subtracted and thresholded from the previous operation of beat frequency calculation) are utilized for wing angle calculation (see Figure 15). As in calculation of wing stroke amplitude, erosion, dilation, and blob detection is performed to determine potentially interesting elements. Prewitt edge detection is performed on the raw side view image to get an understanding of relevant regions (see Figure 16). The edge profile is laid over the blob detected regions and blobs outside of the detected edges are eliminated. This process subtracts all additional sources of noise, and leaves only blobs associated with the wing profile. Centroids of blob trajectories are tracked in subsequent frames to eliminate the effect of occlusions, and to help identify associated blobs in subsequent frames. A line is fitted to the centroids of all blobs for a single wing beat as pictured in Figure 17. The slope of this best fit line determines the wing stroke plane angle. The process is repeated for a number of subsequent wing beats to provide an average and standard deviation of stroke angle. See Figure 22 for a flow chart of the stroke amplitude calculation process.

Figure 15 - Thresholded side image after background subtraction.

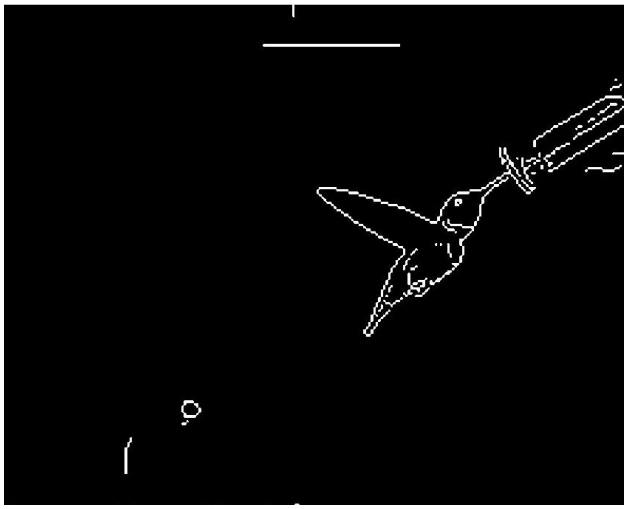

Figure 16 - Prewitt edge detection of raw side image.

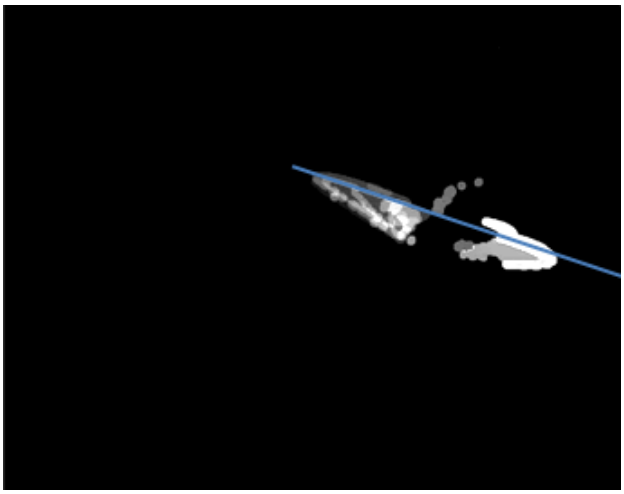

Figure 17 - Edge detected image used to remove extraneous blobs. Remaining blobs tracked and a line fitted to centroids to determine stroke plane angle.

Calculation of body orientation

After performing the previous operations we have a number of components already available for use. Side wing blobs (Figure 17) are subtracted from the side edge detection (Figure 16) to eliminate wings from the body detection (illustrated in Figure 18). Next, stationary components are subtracted from the edge detection leaving only the body (as illustrated in Figure 19). The body edges are treated as a bounding region, and the centroid and orientation can be determined for the resulting blob (see Figure 20). The process is repeated for subsequent frames to get an average and standard deviation of body angle over time. See Figure 24 for a flow chart of the body angle algorithm.

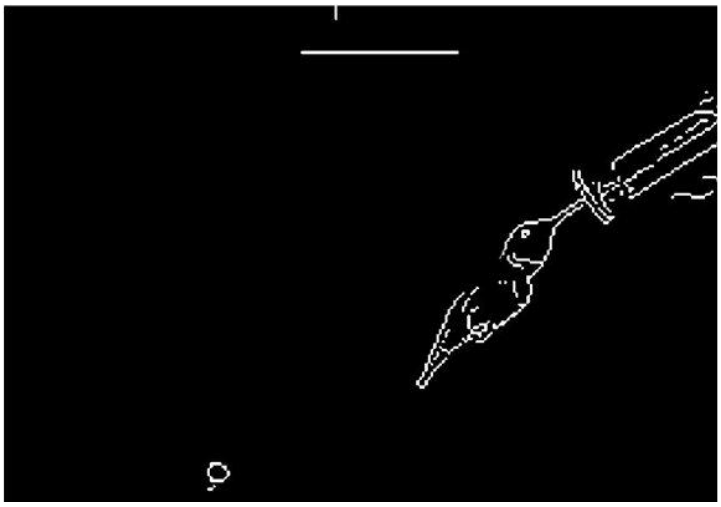

Figure 18 - Wings subtracted from edge detected image.

Figure 19 - Stationary objects subtracted from edge detected image.

Figure 20 - Remaining body treated as single blob. 1st order ellipse fitted to blob, and angle measured.

Results

Flight parameters (beat frequency, body pitch, wing beat amplitude, wing angle of attack) were previously hand calculated for a data set of 12 humming bird videos using techniques described in the literature. The algorithm presented in this work was tested on 12 sets of humming bird hovering data and was shown to calculate similar results (+- 5% of hand calculated values) in most cases. A number of confounding variables (poor video focus, poor lighting conditions, and poorly aligned cameras) were present in the 3 cases that deviated from hand calculated values by more than 5%.

Conclusions

This work is novel in that it fulfills the need for a rapid analysis tool for ornithologists and comparative biologists studying hummingbird flight. The intention of this tool is to transform a pair of high speed video cameras into a rapid diagnostic and analysis tool. Currently a single readily available tool for rapidly determining flight parameters of flying animals does not exist. As a result, there is a temporal and physical disconnect between observation and analysis of bird behaviors. By eliminating hours of labor intensive analysis, it will be possible for researchers to perform experiments and determine experimental viability at a much faster pace.

Suggestions for Future Work

Additional testing should be performed to characterize the reliability of this algorithm before it is used in a research setting. Careful adjustment of focus and lighting conditions will ensure easier analysis by manual and automated techniques.

Figure 21 -Flowchart of beat frequency determination algorithm

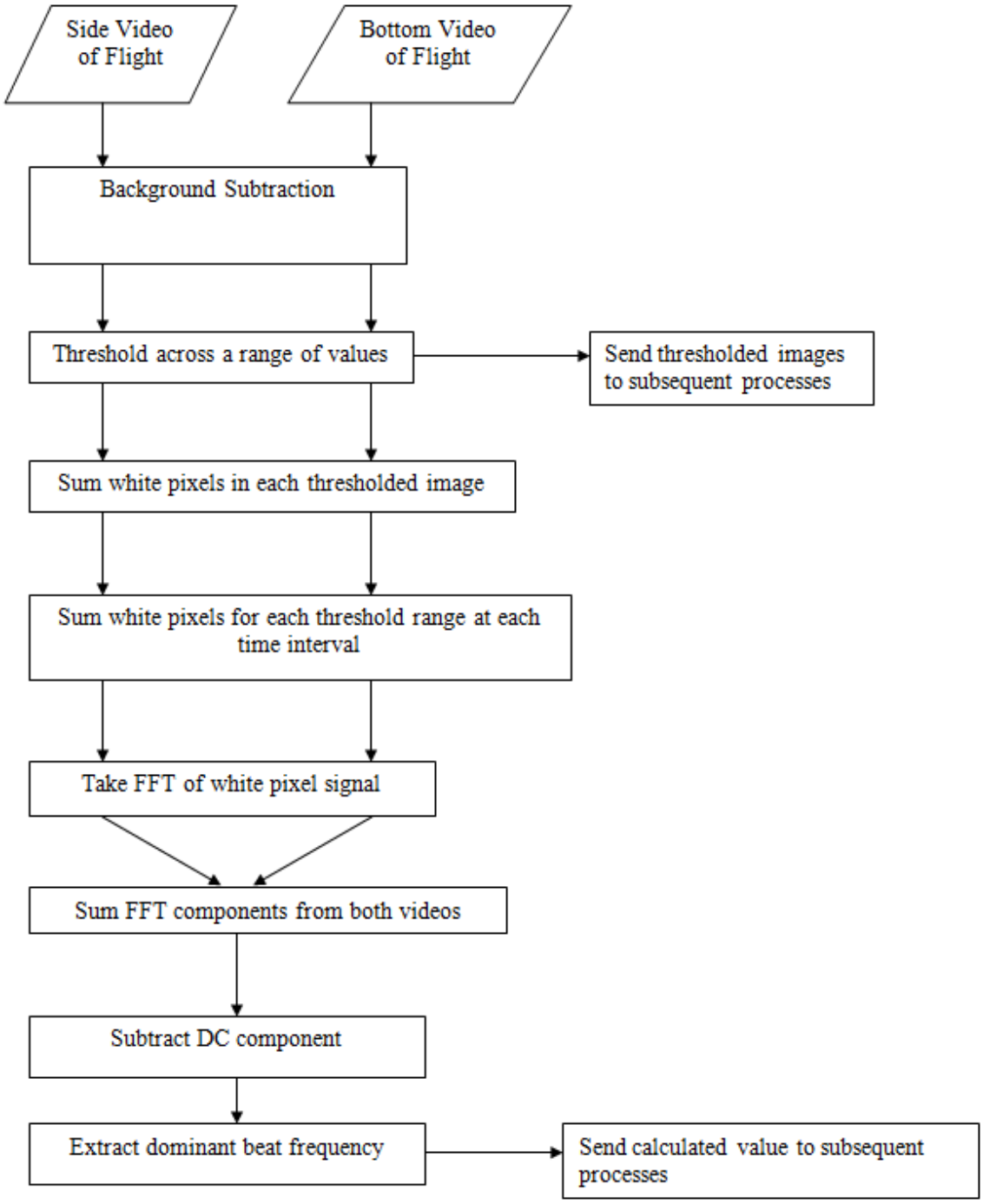

Figure 22 - Flowchart of wing stroke amplitude calculation

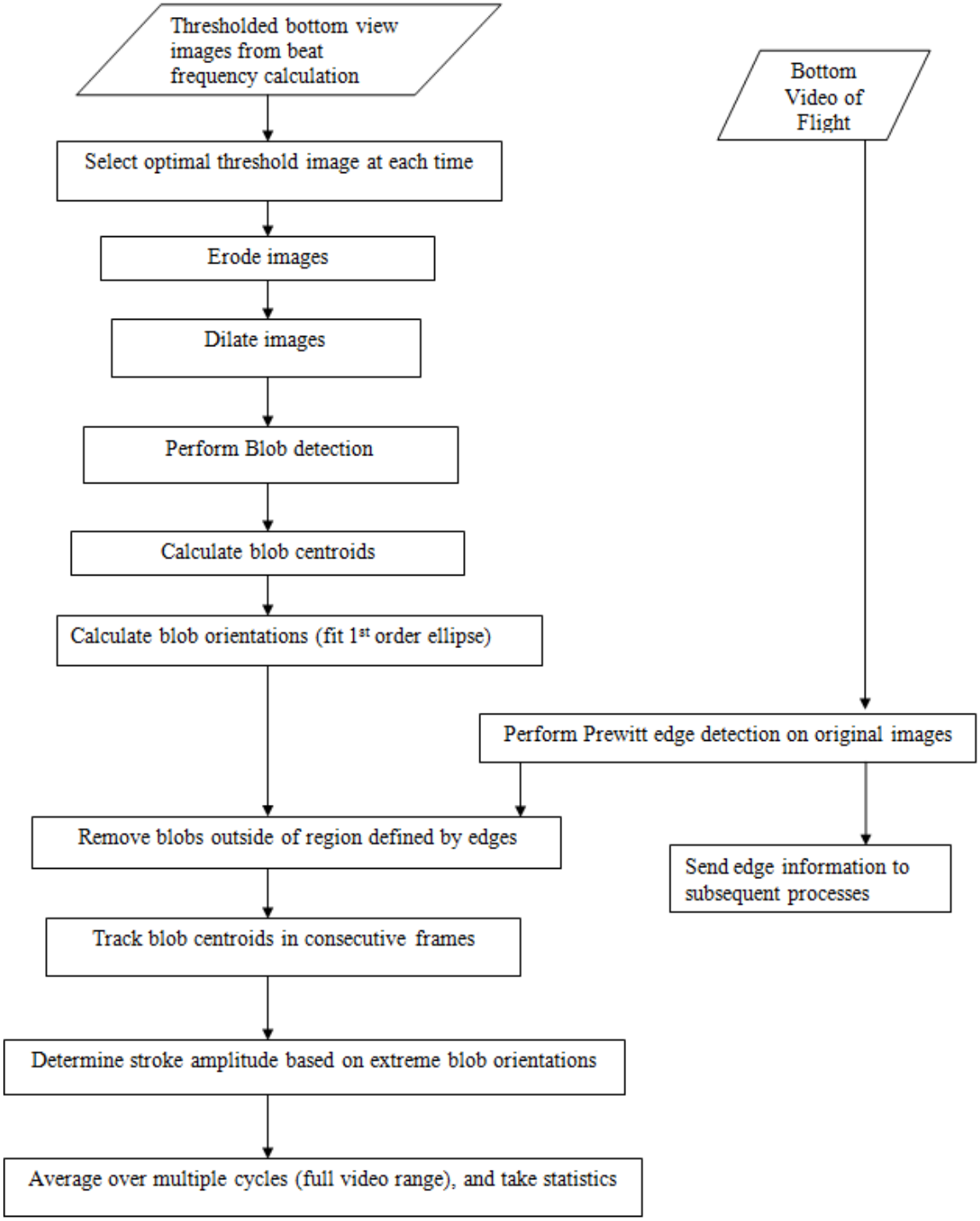

Figure 23- Flowchart of wing angle algorithm

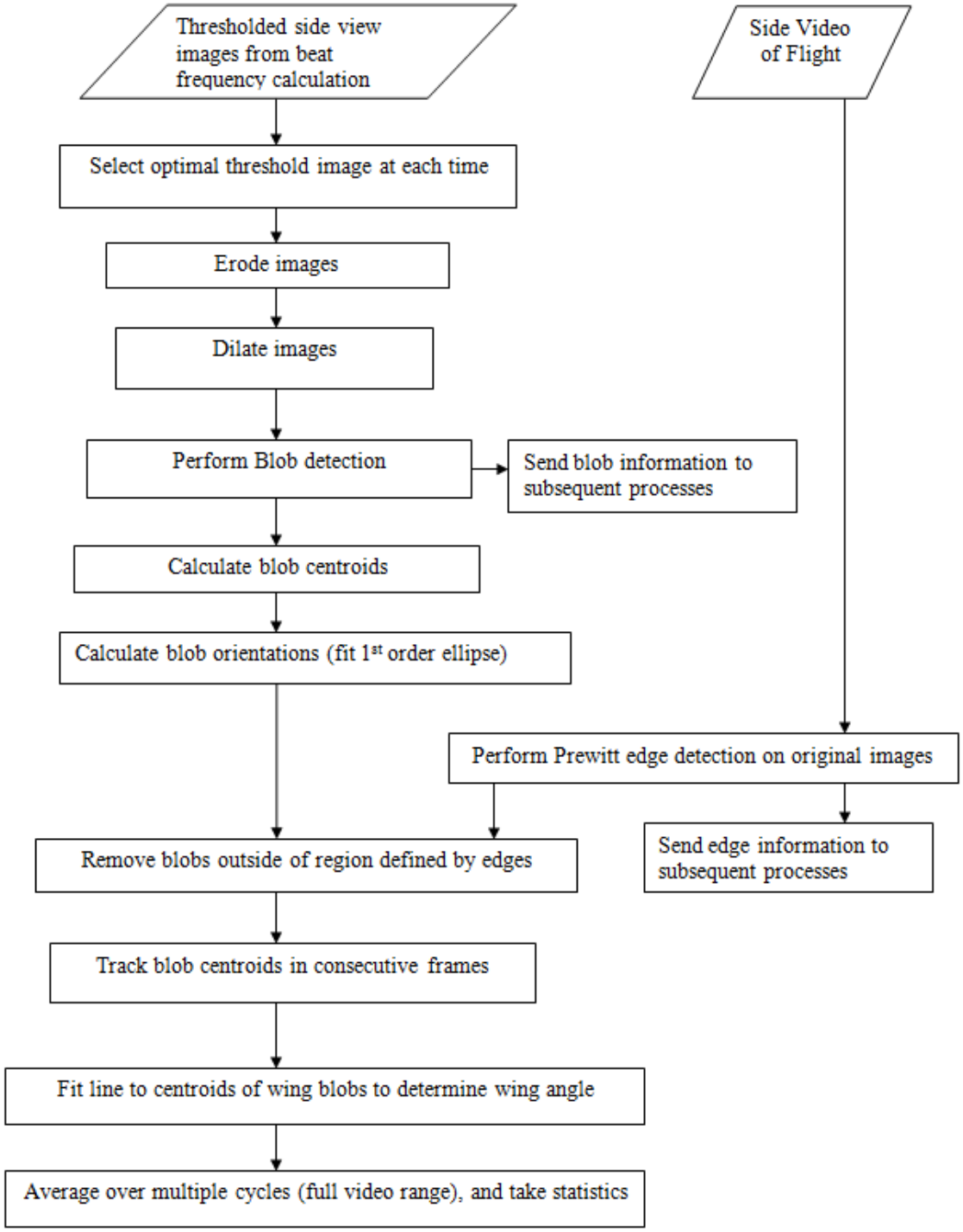

Figure 24- Flowchart of body angle algorithm

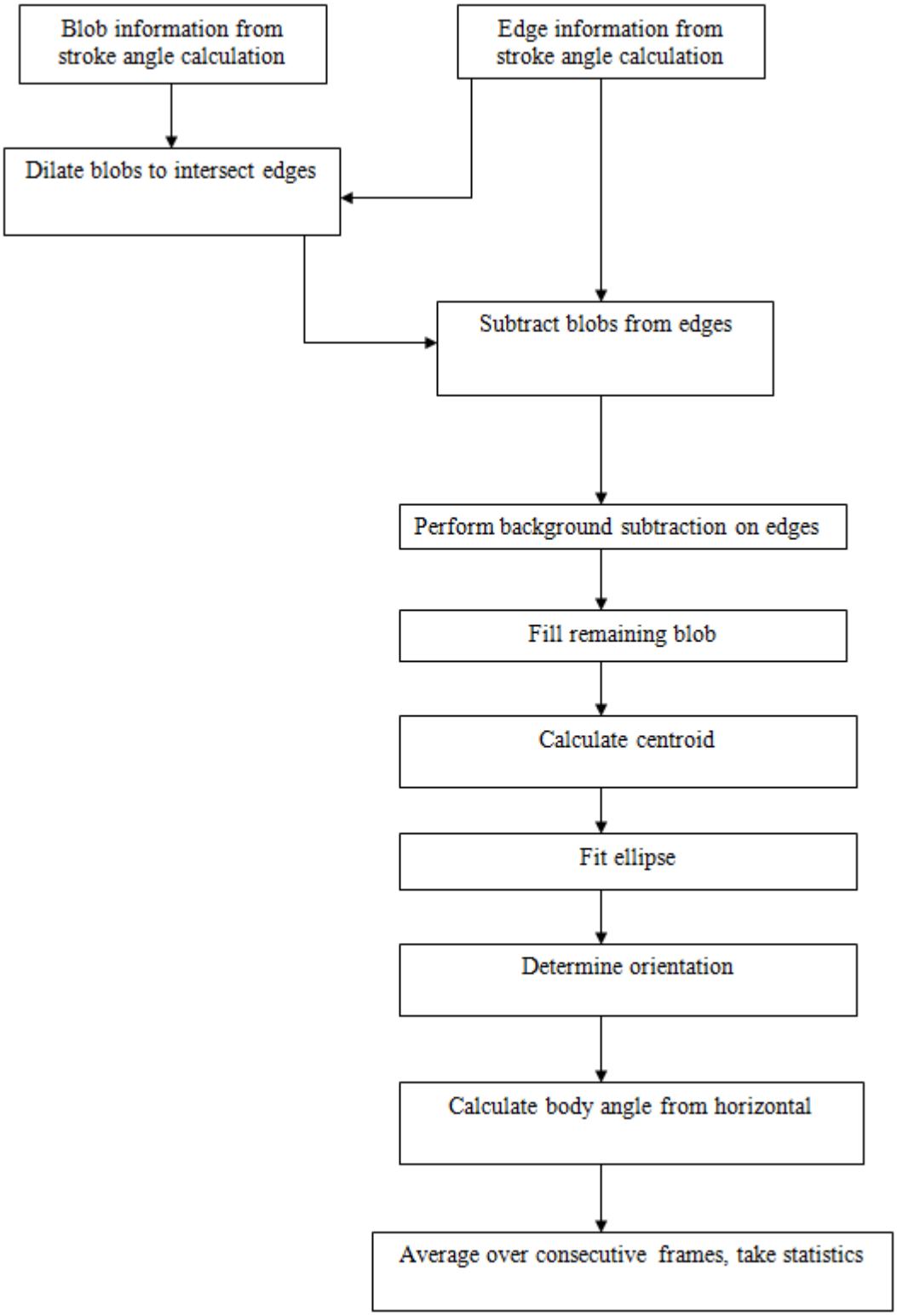

References

[1] Altshuler, D.L. and R. Dudley. (2002). The ecological and evolutionary interface of hummingbird flight physiology. *Journal of Experimental Biology* 205:2325-2336.

[2] Altshuler, D.L. and R. Dudley. (2003). Kinematics of hummingbird hovering flight along simulated and natural elevational gradients. *Journal of Experimental Biology* 206:3139-3147.

[3] Altshuler, D.L., Dudley, R. and C.P. Ellington. (2004). Aerodynamic forces of revolving hummingbird wings and wing models. *Journal of Zoology, London* 264:327-332.

[4] Dudley, R. (1992). Aerodynamics of flight. In: *Biomechanics (Structures & Systems): A Practical Approach* (ed. A.A. Biewener), pp. 97-121. Oxford: Oxford University Press.